

## Article

# Fast Terminal Sliding Mode Control Based on Finite-Time Observer and Improved Reaching Law for Aerial Robots

Pu Yang <sup>\*</sup>, Kejia Feng, Yu Ding  and Ziwei Shen

College of Automation, Nanjing University of Aeronautics and Astronautics, Nanjing 211106, China

<sup>\*</sup> Correspondence: ppyang@nuaa.edu.cn; Tel.: +86-133-3773-5295

**Abstract:** In this paper, a non-singular fast terminal sliding mode control (NFTSMC) strategy based on a finite-time observer and improved reaching rate is proposed to solve the control problem of aerial robot systems subject to actuator faults and internal and external disturbances. Using the control strategy proposed in this paper, rapid convergence and high robustness of the system are guaranteed. In addition, the proposed finite-time observer can observe information related to the actuator fault or internal and external disturbance of the system in an accurate and timely fashion, and actively compensate the fault. The improved reaching law introduced in this paper can cause the system reach the sliding surface quickly, effectively improving the response speed of the system and increasing the tracking performance of the system. The stability of the whole system is proved using Lyapunov stability analysis. Finally, the effectiveness of the proposed control strategy is verified on the basis of a numerical simulation of a six-rotor UAV model with manipulator.

**Keywords:** aerial robot; sliding mode control; finite-time observer; improved reaching law



**Citation:** Yang, P.; Feng, K.; Ding, Y.; Shen, Z. Fast Terminal Sliding Mode Control Based on Finite-Time Observer and Improved Reaching Law for Aerial Robots. *Actuators* **2022**, *11*, 258. <https://doi.org/10.3390/act11090258>

Academic Editor: Giorgio Olmi

Received: 20 August 2022

Accepted: 6 September 2022

Published: 8 September 2022

**Publisher's Note:** MDPI stays neutral with regard to jurisdictional claims in published maps and institutional affiliations.



**Copyright:** © 2022 by the authors. Licensee MDPI, Basel, Switzerland. This article is an open access article distributed under the terms and conditions of the Creative Commons Attribution (CC BY) license (<https://creativecommons.org/licenses/by/4.0/>).

## 1. Introduction

With advances in science and technology, multi-rotor UAVs have been used in various fields, including aerial photography [1], search and rescue [2], and precision agriculture [3]. However, due to design and structural limitations, multi-rotor UAVs cannot come into direct contact with objects in the environment. To solve the problem of interaction with the environment, one or more manipulators can be mounted on UAVs [4,5]. Multi-rotor UAVs with manipulators are called aerial robotic manipulators (AEROMs).

Aerial robotic manipulators have been applied in many fields, such as forest health monitoring and data collection [6], perching in high places and the performance of wall knocking inspection work [7,8]. The ability of aerial robotic manipulators to interact with their environment greatly increases the possibilities of successfully carrying out missions in the air [9].

With the increasing demand for air operations, much research has been performed on the control of aerial robots. However, manipulators exhibit serious coupling interference with multi-rotor UAVs. Therefore, the control problem of aerial robots has always been a focus of research. For example, in [10], an optimization problem control scheme was presented for a crowd of aerial machines performing a search task. In [11], in view of the problem of thrust and joint trajectory control, a control strategy for a multi-bar aerial robot based on motion elements and a nonlinear prediction model was proposed. In [12], an adaptive-repetitive visual-servo controller was proposed to adjust and track the system while solving the control problem arising from the uncertainty of internal and external parameters. Inspired by insect flight, adaptive tracking flight control and iterative learning control algorithms have been proposed to solve dynamic trajectory tracking, unmodeled dynamics, and system errors [13]. In [14], aiming to solve the underactuated problem of an aerial robot composed of a UAV and a manipulator, the researchers proposed a new model-based adaptive motion control algorithm.

Aerial robots are prone to fault problems and external interference during operation. Therefore, it is particularly necessary to design observers to perform timely observation of aerial robots. In [15], in order to solve the problem of precise control of the connecting rod, a low-latitude estimator with a nonlinear high-gain observation period was proposed that was able to determine the state of the whole system from the sensor. In [16], in order to solve the problem of interference hindering the completion of the task in n-order robot manipulators, the researchers used the robust position input observer to obtain a decoupling estimation from the unknown interference. The observer displayed good results. In addition to external disturbances, there are many uncertainties in UAV systems. In [17], a control strategy based on an adaptive sliding-mode disturbance observer was proposed for UAV systems subjected to external disturbance and uncertainty. The proposed observer effectively estimated and compensated for external disturbances and state-dependent uncertainties. In [18], the researchers extended the concept of the wrench observer to a tilted six-rotor UAV with a 3-DOF manipulator to estimate progress and robustness to measurement noise.

At present, due to their simplicity of design, the design of controllers for aerial robots mostly consists of the improvement and extension of PID controllers [19–22]. However, there are many control technologies with better control performance. In [23], an adaptive fault-tolerant scheme based on a frequency domain identification state space model was proposed for the actuator failure of a ducted-fan aerial robot. In [24], in order to solve the visual servo problem of a restricted mobile robot, a nonlinear model predictive control based on the Gaussian process was proposed. Compared with PID control, backstepping control has better performance for uncertain and parametric systems. In [25], the researchers combined backstepping control with the cuckoo search algorithm to track the trajectory of aerial robots, reducing the stability time and overshoot of the system.

In complex systems, sliding mode control has strong robustness to system faults, uncertainties and disturbances. Therefore, sliding mode control has also been promoted in the field of aerial robots. In [26], a high-order sliding mode controller was developed to counteract the influence of overhang on the rotor UAV, and a super twisting control input was generated to suppress load swing. In [27], a non-singular terminal sliding mode controller was designed using time-delay estimation, providing higher control precision than the proportional differential. In [28], A hybrid algorithm for the optimization of sliding mode control theory was proposed, verifying the effectiveness of the autonomous operation of an aerial robot over a paddy field.

The above investigations indicate that aerial robot systems are a highly coupled and underactuated system. Uncertainties, faults, and disturbances in the system will have a serious influence. There have been certain studies on the uncertainties and external interference to which aerial robots are subjected, but there have been few studies on actuator failure in aerial robots. Similarly, there have been few studies on the suppression of chattering in aerial robot control.

The shortcomings of previous research can be summarized as being related to three aspects. Firstly, some methods combine sliding mode control with other control methods to produce a complex controller, and this control strategy has certain limitations in practical application. Second, some methods are very sensitive to interference and uncertainty, adding unnecessary restrictions or too many parameters in the design. Finally, some methods do not effectively solve the chattering problem of the system. On the basis of existing research, the trajectory tracking control problem of aerial robot systems subject to actuator failure and internal and external disturbances is studied using a non-singular terminal sliding mode control algorithm based on a finite-time observer and an improved reaching law. The main novelty and characteristics of this paper can be summarized as follows:

- (1) A finite-time observer based on terminal sliding mode is designed by separating the fault of the aerial robot system from the internal and external unknown disturbances. The finite time lumped estimation and compensation of actuator fault information and internal and external disturbances are realized without obtaining the upper bound of disturbance.
- (2) Based on the non-singular terminal sliding surface, an improved reaching law is introduced that enables the system to reach the sliding surface in a finite amount of time. This improves the robustness of the system and effectively reduces the chattering phenomenon.
- (3) The model studied in this paper considers the effects of actuator failure, manipulator action interference, and unknown external interference on the aerial robot system, thus improving the effectiveness and availability of the control algorithm.

The remainder of this paper is organized as follows: the models and problem descriptions of aerial robot systems are given in Section 2. Section 3 presents the design of the finite-time observer. In Section 4, the detailed design process of the NFTSM controller based on the improved reaching law and the finite-time observer is given. The corresponding simulation results are provide in Section 5 in order to demonstrate the effectiveness of the proposed control strategy. Finally, the contents of this paper are summarized, and future research directions are given.

## 2. System Model Description

The schematic diagram of the aerial robot system is shown in Figure 1. The aerial robot system is composed of a six-propeller aircraft and a two-degree-of-freedom manipulator. A six-rotor UAV was selected because of its strong load capacity, which has great application for air operations. It provides a light arm for the system, thereby increasing flight autonomy. Although it moves in the  $X_v O_v Z_v$  plane, the manipulators attached to the UAV can interact with objects in 3D space. In the following section, the system is divided into two subsystems, namely, the UAV and the manipulator, for the purposes of dynamic modeling. This overall method regards the coupling problem as an internal interference problem [29].

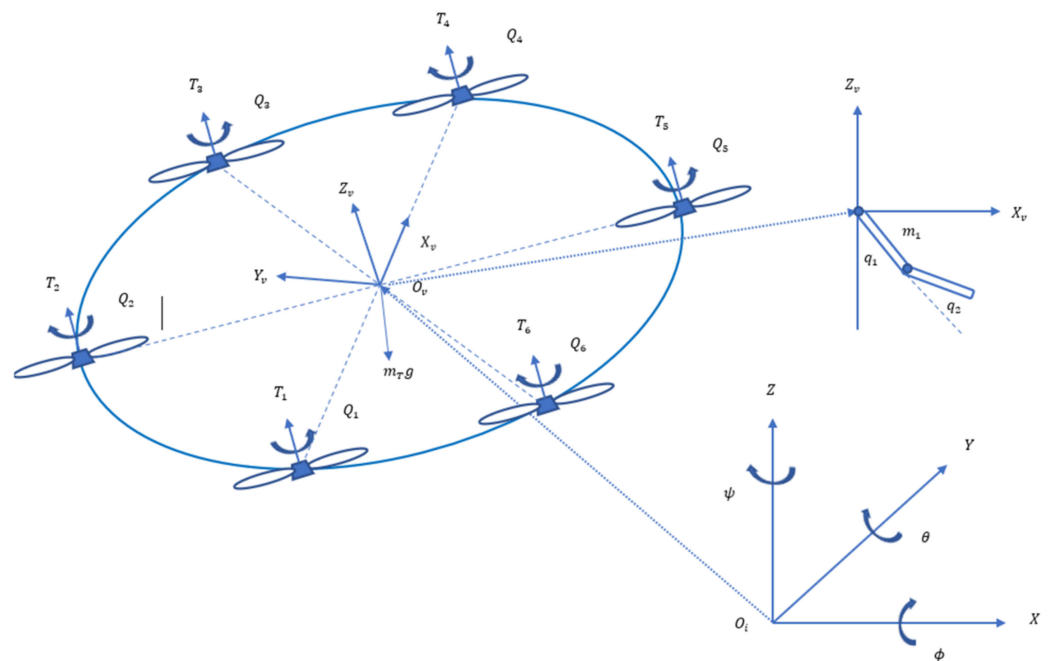


Figure 1. Model of aerial robot.

### 2.1. Kinematics of Six-Rotor Aircraft

The six-rotor UAV is a rigid body and is affected by external forces exerted on its centroid. Following the method described in [30], Newton's law, the Euler–Lagrange equation and small-angle simplification are used. The dynamic model equation of the six-rotor UAV is shown below:

$$\begin{cases} \ddot{x} = (\sin \psi \sin \phi + \cos \psi \sin \theta \cos \phi) \frac{U_z}{m} \\ \ddot{y} = (\sin \psi \sin \theta \cos \phi - \cos \psi \sin \phi) \frac{U_z}{m} \\ \ddot{z} = (\cos \theta \cos \phi - g) \frac{U_z}{m} \\ \ddot{\phi} = \frac{I_{yy} - I_{zz}}{I_{xx}} (\dot{\theta} \dot{\psi}) - \frac{J_r}{I_{xx}} \dot{\theta} \Omega_r + \frac{U_\phi}{I_{xx}} \\ \ddot{\theta} = \frac{I_{zz} - I_{xx}}{I_{yy}} (\dot{\phi} \dot{\psi}) + \frac{J_r}{I_{yy}} \dot{\phi} \Omega_r + \frac{U_\theta}{I_{yy}} \\ \ddot{\psi} = \frac{I_{xx} - I_{yy}}{I_{zz}} (\dot{\phi} \dot{\theta}) + \frac{U_\psi}{I_{zz}} \end{cases} \quad (1)$$

where  $\ddot{x}, \ddot{y}, \ddot{z}$  denotes the linear acceleration in the position subsystem;  $\ddot{\phi}, \ddot{\theta}, \ddot{\psi}$  represents the angular acceleration of the attitude system in the rotor UAV;  $m$  represents the quality of the unmanned aerial vehicle;  $U_z, U_\phi, U_\theta, U_\psi$  represents the torque produced by the six propellers, defined as  $U_z = (T_1 + T_2 + T_3 + T_4 + T_5 + T_6)$ ,  $T_n$  represents the force generated by propeller  $n$ ,  $U_\phi = \frac{l\sqrt{3}}{2}(-T_2 - T_3 + T_5 + T_6)$ ,  $U_\theta = \frac{l}{2}(2T_1 + T_2 - T_3 - 2T_4 - T_5 + T_6)$ ,  $U_\psi = (Q_1 - Q_2 + Q_3 - Q_4 + Q_5 - Q_6)$ , where  $Q_n$  is the torque caused by propeller  $n$ ,  $l$  represents the distance from the rotor to the centroid;  $I_{xx}, I_{yy}, I_{zz}$  is the main inertia moment of the rotor UAV; and  $\Omega_r = \sum_{i=1}^6 \omega_i$ ,  $\omega_i$  represents the speed of the  $i$  motor.

### 2.2. Dynamic Model of Manipulator

The two-degree-of-freedom manipulator is suspended on the lower hanging plate of the aircraft pod, and the manipulator moves in the  $X_v O_v Z_v$  plane. The other degrees of freedom can be realized by the attitude transformation of the UAV, so the design can realize the function of interaction with objects in three-dimensional space required by the flying robot. The transmission of torque is realized by flexible rope traction, and the inertia ratio of the joints is decreased. By introducing Newton–Euler method [31], the dynamic model is derived as follows:

$$\ddot{q} = M^{-1}(q)(\tau - C(q, \dot{q})\dot{q} - Gq - F(\dot{q})) \quad (2)$$

where  $M \in R^{2 \times 1}$  represents the inertial matrix of the system;  $q, \dot{q}$  and  $\ddot{q}$  are joint vector, joint angular velocity vector, and joint angular acceleration vector, respectively;  $C \in R^{2 \times 2}$  represents the coriolis and centrifugal force matrix; and  $\tau = [\tau_1, \tau_2]^T \in R^{2 \times 1}$  represents joint torque. The selection of aerial manipulator should meet the requirements of light weight and slenderness, such that the mass of the manipulator can be concentrated on the joint, and the quality of the connecting rod of the manipulator is not considered.

Then, when the gravity of the manipulator and the torque at the joint are brought into the model of the aircraft as disturbance and disturbance torque, we can obtain:

$$\begin{cases} \ddot{x} = (\sin \psi \sin \phi + \cos \psi \sin \theta \cos \phi) \frac{U_z}{m_T} \\ \ddot{y} = (\sin \psi \sin \theta \cos \phi - \cos \psi \sin \phi) \frac{U_z}{m_T} \\ \ddot{z} = (\cos \theta \cos \phi - g) \frac{U_z}{m_T} \\ \ddot{\phi} = \frac{I_{yy} - I_{zz}}{I_{xx}} (\dot{\theta} \dot{\psi}) - \frac{J_r}{I_{xx}} \dot{\theta} \Omega_r + \frac{U_\phi}{I_{xx}} \\ \ddot{\theta} = \frac{I_{zz} - I_{xx}}{I_{yy}} (\dot{\phi} \dot{\psi}) + \frac{J_r}{I_{yy}} \dot{\phi} \Omega_r + \frac{U_\theta}{I_{yy}} + \tau_1 + \tau_2 \\ \ddot{\psi} = \frac{I_{xx} - I_{yy}}{I_{zz}} (\dot{\phi} \dot{\theta}) + \frac{U_\psi}{I_{zz}} \end{cases} \quad (3)$$

where  $m_r = m + m_1$ ,  $m_r$  is the total mass of the system, and  $m_1$  is the mass of the manipulator; and  $\tau_1, \tau_2$  denotes the moment of the two joints acting on the aircraft.

**Remark 1.** The motion of the manipulator is only carried out in the  $X_vO_vZ_v$  plane of the system, and the generated torque effect is regarded as only affecting the pitch angle of the system.

### 2.3. Problem Description

For aerial robot systems, actuator failures and external disturbances are inevitable, so in this part, actuator failures and external disturbances are introduced into the system model. The actuator failure type is the loss of control effectiveness [32]. The system failure and disturbance model can be described as follows:

$$\begin{cases} \dot{x}_{11} = x_{12} \\ \dot{x}_{12} = \frac{1}{m_T}(1 - \mu_1)U_1 + d_1 \\ \dot{x}_{21} = x_{22} \\ \dot{x}_{22} = \frac{1}{m_T}(1 - \mu_2)U_2 + d_2 \\ \dot{x}_{31} = x_{32} \\ \dot{x}_{32} = \frac{1}{m_T}(1 - \mu_3)U_3 + d_3 \end{cases} \quad (4)$$

$$\begin{cases} \dot{x}_{41} = x_{42} \\ \dot{x}_{42} = \frac{I_{yy} - I_{zz}}{I_{xx}}x_{52}x_{62} - \frac{J_r}{I_{xx}}\Omega_r x_{52} + \frac{1 - \mu_4}{I_{xx}}U_\phi + d_\tau + d_4 \\ \dot{x}_{51} = x_{52} \\ \dot{x}_{52} = \frac{I_{zz} - I_{xx}}{I_{yy}}x_{42}x_{62} + \frac{J_r}{I_{yy}}\Omega_r x_{42} + \frac{1 - \mu_5}{I_{yy}}U_\theta + d_5 \\ \dot{x}_{61} = x_{62} \\ \dot{x}_{62} = \frac{I_{xx} - I_{yy}}{I_{zz}}x_{42}x_{52} + \frac{1 - \mu_6}{I_{zz}}U_\psi + d_6 \end{cases} \quad (5)$$

where  $x_{i1} = (x, y, z, \phi, \theta, \psi)^T$ ,  $x_{i2} = (\dot{x}, \dot{y}, \dot{z}, \dot{\phi}, \dot{\theta}, \dot{\psi})^T$ ,  $d_i (i = 1, 2, \dots, 6)$  represents an external disturbance to the system, and  $d_\tau = \tau_1 + \tau_2$  represents the disturbance caused by manipulator action, and these are collectively referred to as disturbance terms in the following.  $U_i$  represents the virtual input control of the system:

$$\begin{cases} U_1 = (\sin \psi \sin \phi + \cos \psi \sin \theta \cos \phi)U_z \\ U_2 = (\sin \psi \sin \theta \cos \phi - \cos \psi \sin \phi)U_z \\ U_3 = (\cos \theta \cos \phi - g)U_z \end{cases} \quad (6)$$

where  $\mu_i$  represents the effectiveness of actuator operation, whereby  $\mu_i = 0$  represents the normal operation of the actuator, in which the input of the corresponding control channel is not affected. When  $\mu_i = 1$ , this indicates that the actuator has been completely destroyed, and the input of the corresponding control channel is zero. When  $0 < \mu_i < 1$ , this indicates that part of the actuator has failed, resulting in lack of input.

The purpose of this paper is to design a fault-tolerant controller for a flight robot system subject to actuator failures and internal and external disturbances. For this purpose, the following are some reasonable assumptions and lemmas:

**Assumption 1.** Although the external disturbance of the system is unknown, since the external disturbance is always limited, the external disturbance is bounded:  $|d_i| \leq D_i, (i = 1, 2, 3 \dots 6)$ .

**Assumption 2.** Due to the limited power of the manipulator movement, the internal disturbance torque generated by the action of the manipulator in the system is bounded:  $|d_\tau| \leq D_\tau$ . Combined with Assumption 1, the internal and external disturbances are integrated into one, and the total disturbance of the system can be obtained as follows:  $D(t) = [d_1, d_2, d_3, d_4 + d_\tau, d_5, d_6]^T$ ; therefore,  $\|D(t)\| \leq D_i + D_\tau$ .

**Lemma 1 ([33]).** A state description system is as follows:

$$\dot{x}(t) = f(x), x(0) = x_0 \quad (7)$$

where  $f(x) : R_+ \times R^n \rightarrow R^n$ . If there exists a positive definite function  $V(x)$  which satisfies:

$$\dot{V}(x) \leq -\alpha V^p(x) - \beta V^q(x) \quad (8)$$

where  $\alpha > 0, \beta > 0, 0 < p < 1$  and  $q > 1$ , then the original system can converge in finite time  $T$ , and  $T$  satisfies:

$$T \leq T_{max} = \frac{1}{\alpha(1-p)} + \frac{1}{\beta(q-1)} \quad (9)$$

**Lemma 2 ([34]).** For the following improved reaching law:

$$\begin{cases} \dot{s} = -\frac{k}{\Phi(s)} |s|^\alpha \text{sgn}(s) \\ \Phi(s) = \eta + \xi \left(1 + \frac{|s|^{1-\alpha}}{v}\right)^{-1} \end{cases} \quad (10)$$

where  $0 < \alpha < 1, \eta > 0, \xi > 0, \xi + \eta < 1, |\cdot|$  represents the absolute value of a function.  $k > 0$ , represents the coefficient of the reaching law.  $v = \sigma |s_0|^{1-\alpha}, \sigma > 0, s_0$  represents the initial value of the switching function.

Then, the reaching law can cause the system to reach the sliding mode surface in a finite time  $t_r$ , and can effectively suppress system chattering.

$$t_r = \frac{|s_0|^{1-\alpha}}{k(1-\alpha)} \left[ \eta + \xi(1-\alpha)^2 \sigma \ln \left(1 + \frac{1}{\sigma}\right) \right] \quad (11)$$

where  $s_t = 0$ ,  $t_r$  represents the time at which the switching function first reaches the sliding surface.

### 3. Design of the Fault and Disturbance Observer

In this part, in order to obtain accurate fault information regarding the system, including information on the actuator and internal and external disturbances, and to perform timely compensation, a finite-time observer is designed for System (5). Equations (4) and (5) can be rewritten as the following state equations:

$$\begin{cases} \dot{X}_1(t) = X_2(t) \\ \dot{X}_2(t) = F(X_2) + G(I - E)U(t) + D(t) \end{cases} \quad (12)$$

where  $X_1(t)$  and  $X_2(t)$  represent the state vector of the system,  $U(t)$  is the input vector of the system,  $G$  represents the control effectiveness matrix,  $I \in R^{6 \times 6}$  is the unit matrix,  $E = \text{diag}\{\mu_1, \mu_2, \mu_3, \mu_4, \mu_5, \mu_6\}$  represents the fault efficiency of the actuators, and  $D(t)$  represents the aggregation of the internal and external disturbances of the system.

In order to obtain accurate fault information and perform timely compensation, a finite-time observer is designed for System (12). The unknown items are separated from the formula and rewritten as follows:

$$\begin{cases} \dot{X}_2(t) = -l_1 X_2 + GU(t) + D^* \\ D^* = l_1 X_2 + F(X_2) + \gamma \\ \gamma = D(t) - GEU(t) \end{cases} \quad (13)$$

where  $l_1 > 0$  is the vector of gain constants,  $D^*$  represents the introduced intermediate variable, the actuator failure fault and internal and external interference of the system are

combined into  $\gamma = [\gamma_1, \gamma_2, \gamma_3, \gamma_4, \gamma_5, \gamma_6]^T$ , which represents the collection of all system uncertainties. The auxiliary systems are established as follows:

$$\dot{\hat{X}}_2(t) = -l_1 \hat{X}_2 + GU(t) \tag{14}$$

Definition error is  $X_e = X_2 - \hat{X}_2$ . With simple calculations:

$$\dot{X}_e = -l_1 X_e + D^* \tag{15}$$

$D^*$  is set as an input to the corresponding observer, as follows:

$$\begin{cases} \dot{X}_e = -l_2 \hat{X}_e + \dot{X}_e + l_2 X_e + l_3 \text{sign}^{\frac{\lambda_1}{\lambda_2}}(\tilde{X}_e) + l_4 \text{sign}^{\frac{\lambda_2}{\lambda_1}}(\tilde{X}_e) \\ \hat{D}^* = l_1 \hat{X}_e + \dot{X}_e \end{cases} \tag{16}$$

where  $\hat{D}^* = [\hat{d}_1^*, \hat{d}_2^*, \hat{d}_3^*, \hat{d}_4^*, \hat{d}_5^*, \hat{d}_6^*]^T$  represents the observed value of  $D^*$ ,  $\tilde{X}_e = X_e - \hat{X}_e$  is the observation error,  $l_2, l_3$  and  $l_4$  are positive constants indicating gains,  $\text{sign}^p(x) = \text{sign}(x) * |x|^p$ ,  $\text{sign}^p(X) = [\text{sign}^p(x_1), \text{sign}^p(x_2), \dots, \text{sign}^p(x_n)]^T$ , where  $\text{sign}(\cdot)$  represents a symbolic function, and  $\lambda_1$  and  $\lambda_2$  are two positive odd numbers, and satisfy  $\lambda_1 < \lambda_2$ .

**Theorem 1.** For the aerial robot system described in Equation (12), an observer is designed in Equation (16) that is able to accurately estimate the value of the uncertainty term  $\gamma$  in a finite amount of time.

**Proof of Theorem 1.** Combining (13) and (14), we can obtain:

$$\begin{aligned} \dot{\tilde{X}}_e &= \dot{X}_e + l_2 \hat{X}_e - \dot{X}_e - l_2 X_e - l_3 \text{sign}^{\frac{\lambda_1}{\lambda_2}}(\tilde{X}_e) - l_4 \text{sign}^{\frac{\lambda_2}{\lambda_1}}(\tilde{X}_e) \\ &= -l_2 \tilde{X}_e - l_3 \text{sign}^{\frac{\lambda_1}{\lambda_2}}(\tilde{X}_e) - l_4 \text{sign}^{\frac{\lambda_2}{\lambda_1}}(\tilde{X}_e) \end{aligned} \tag{17}$$

A Lyapunov function is selected as follows:

$$V_x = \frac{1}{2} \tilde{X}_e^T \tilde{X}_e \tag{18}$$

According to Formula (18):

$$\begin{aligned} \dot{V}_x &= \tilde{X}_e^T \dot{\tilde{X}}_e \\ &= -\tilde{X}_e^T (l_2 \tilde{X}_e + l_3 \text{sign}^{\frac{\lambda_1}{\lambda_2}}(\tilde{X}_e) + l_4 \text{sign}^{\frac{\lambda_2}{\lambda_1}}(\tilde{X}_e)) \\ &= -l_2 2V_x - l_3 (2V_x)^{\frac{\lambda_1 + \lambda_2}{2\lambda_2}} - l_4 (2V_x)^{\frac{\lambda_1 + \lambda_2}{2\lambda_1}} \leq -\rho_1 V_x^{\frac{\lambda_1 + \lambda_2}{2\lambda_2}} - \rho_2 V_x^{\frac{\lambda_1 + \lambda_2}{2\lambda_1}} \leq 0 \end{aligned} \tag{19}$$

where  $\rho_1 = 2^{\frac{\lambda_1 + \lambda_2}{2\lambda_2}} * l_3, \rho_2 = 2^{\frac{\lambda_1 + \lambda_2}{2\lambda_1}} * l_4$ ,  $\lambda_1$  and  $\lambda_2$  are two positive numbers, and satisfy  $\lambda_1 < \lambda_2$ . We can obtain that  $0 < \frac{\lambda_1 + \lambda_2}{2\lambda_2} < 1$  and  $1 < \frac{\lambda_1 + \lambda_2}{2\lambda_1}$ . Therefore, according to Lemma 1, the observation error  $\tilde{X}_e$  converges in a finite amount of time  $T_x$ , where:

$$T_x = \frac{\lambda_2 - \lambda_1}{2\rho_1 \lambda_2} + \frac{\lambda_2 - \lambda_1}{2\rho_2 \lambda_1} \tag{20}$$

Then, combining Formulas (15) and (16), we can obtain:

$$\hat{D}^* = -l_1 \tilde{X}_e + D^* \tag{21}$$

Therefore, when  $\tilde{X}_e$  converges, the observed value of  $D^*$  is also the same as its actual value, and then, according to Equation (13), an accurate value of the uncertainty  $\gamma$  can be obtained as follows:

$$\hat{\gamma} = \hat{D}^* - l_1 \hat{X}_2 - F(\hat{X}_2) \quad (22)$$

Theorem 1 has been proved.  $\square$

**Remark 2.** In Formula (16),  $\dot{X}_e$  is needed to realize the designed observer. To meet this requirement, the high-order sliding mode differentiator designed in [34] is introduced. After inputting the signal value  $X_e$ , the specific value of  $\dot{X}_e$  can be obtained in a finite amount of time.

**Remark 3.** According to the above proof, it can be considered that the value of the system uncertainty observed by the finite-time observer is equal to the actual fault of the system.

#### 4. Design of Fault-Tolerant Controller

In this section, a TSMC control method based on an improved reaching law is proposed that can be used in aerial robot systems subject to actuator faults and internal and external disturbances. The main advantage of this control algorithm is that, in the case of actuator faults and internal and external disturbances, the system possesses rapid convergence speed, strong robustness, and the ability to effectively suppress chattering.

For the design of the system controller, the position input and output channels can be regarded as independent, so the controller is designed with control channel 1 as an example to show the details of the controller design process. To facilitate the design of the display controller, control channel 1 in Formula (12) is written as follows:

$$\ddot{x}_1 = f_1 + g_1 u_1 + \gamma_1 \quad (23)$$

where  $\ddot{x}_1$  represents the state of system control channel 1,  $f_1, g_1$  are known functions of the system, and  $\gamma_1$  is the set of uncertainties in control channel 1. Tracking error is defined as:

$$e_1 = x_{1d} - x_1 \quad (24)$$

where  $e_1, x_{1d}, x_1$  represent tracking error, target value, and system state, respectively.

The terminal sliding surface is designed as follows:

$$s_1 = e_1 + k_1 |e_1|^{a_1} \text{sgn}(e_1) + k_2 |\dot{e}_1|^{a_2} \text{sgn}(\dot{e}_1) \quad (25)$$

where  $e_1, \dot{e}_1$  are the first derivative of error and error, respectively,  $\text{sgn}(\cdot)$  is the symbolic function,  $k_1, k_2$  are controller parameters greater than zero, and  $1 < a_2 < a_1 < 2$  is the design parameter.

By calculating the first-order derivative of (25) and combining (23) and (24), we can obtain:

$$\begin{aligned} \dot{s}_1 &= \dot{e} + k_1 a_1 |e_1|^{a_1-1} \dot{e}_1 + k_2 a_2 |\dot{e}_1|^{a_2-1} \ddot{e}_1 \\ &= \dot{e} + k_1 a_1 |e_1|^{a_1-1} \dot{e} + k_2 a_2 |\dot{e}_1|^{a_2-1} (\ddot{x}_{1d} - f_1 - g u + \gamma_1) \end{aligned} \quad (26)$$

In combination with Lemma 2, the controller can be designed as:

$$u_1 = \frac{1}{g_1} \left\{ \ddot{x}_{1d} - f_1 - \hat{\gamma}_1 + \frac{k |s_1|^\alpha \text{sgn}(s_1)}{k_2 a_2 |\dot{e}_1|^{a_2-1} \left[ \eta + \xi \left( 1 + \frac{|s_1|^{1-\alpha}}{\nu} \right)^{-1} \right]} + \frac{\dot{e} + k_1 a_1 |e_1|^{a_1-1} \dot{e}}{k_2 a_2 |\dot{e}_1|^{a_2-1}} \right\} \quad (27)$$

where  $\hat{\gamma}_1$  represents the estimated value of the accumulated uncertainty for system control channel 1, which can be calculated using Formula (22).

**Theorem 2.** For aerial robot systems subject to actuator faults and internal and external disturbances, as described by Formula (12), the controller (27) designed in this paper can cause the system state to converge and reach the sliding surface in a finite amount of time. It is also able to suppress system chattering.

**Proof of Theorem 2.** Firstly, it will be proved that the sliding surface can be reached in a finite amount of while, and that chattering can be suppressed:

According to Formula (10), we can get:

$$-kdt = \left[ \eta + \zeta \left( 1 + \frac{|s|^{1-\alpha}}{\nu} \right)^{-1} \right] |s|^{-\alpha} \text{sign}(s) \tag{28}$$

when  $s > 0$ ,

$$\begin{aligned} t_r &= -\frac{1}{k} \int_{s_0}^{s_t} \left[ \eta + \zeta \left( 1 + \frac{|s|^{1-\alpha}}{\nu} \right)^{-1} \right] |s|^{-\alpha} \text{sign}(s) ds \\ &= -\frac{1}{k} \int_{s_0}^{s_t} \eta s^{-\alpha} ds - \frac{1}{k} \int_{s_0}^{s_t} \zeta \left( 1 + \frac{s^{1-\alpha}}{\nu} \right)^{-1} s^{-\alpha} ds \end{aligned} \tag{29}$$

where

$$\begin{aligned} \int_{s_0}^{s_t} \zeta \left( 1 + \frac{s^{1-\alpha}}{\nu} \right)^{-1} s^{-\alpha} ds &= (1 - \alpha) \int_{s_0}^{s_t} \frac{\zeta \nu}{\nu + s^{1-\alpha}} d(s^{1-\alpha}) \\ &= (1 - \alpha) \int_{\beta_0}^{\beta_t} \frac{\zeta \nu}{\nu + \beta} d\beta \\ &= \zeta \nu (1 - \alpha) \ln(\nu + \beta) \Big|_{\beta_0}^{\beta_t} \\ &= \zeta \nu (1 - \alpha) \ln(\nu + s^{1-\alpha}) \Big|_{s_0}^{s_t} \end{aligned} \tag{30}$$

then,

$$\begin{aligned} t_r &= -\frac{1}{k} \left( \frac{\eta}{1-\alpha} s_0^{1-\alpha} \Big|_{s_0}^{s_t} + \zeta \nu (1 - \alpha) \ln(\nu + s^{1-\alpha}) \Big|_{s_0}^{s_t} \right) \\ &= \frac{1}{k} \left( \frac{\eta}{1-\alpha} s_0^{1-\alpha} + \zeta \nu (1 - \alpha) \ln(\nu + s_0^{1-\alpha}) \right) - \frac{\zeta \nu (1-\alpha) \ln(\nu)}{k} \\ &= \frac{1}{k} \left[ \frac{\eta}{1-\alpha} s_0^{1-\alpha} + \zeta \nu (1 - \alpha) \ln \left( 1 + \frac{s_0^{1-\alpha}}{\nu} \right) \right] \end{aligned} \tag{31}$$

when  $s < 0$ ,

$$t_r = \frac{1}{k} \left( \frac{\eta}{1-\alpha} (-s)^{1-\alpha} + \zeta \nu (1 - \alpha) \ln \left( 1 + \frac{(-s)^{1-\alpha}}{\nu} \right) \right) \tag{32}$$

Combining Equations (31) and (32), we can obtain:

$$t_r = \frac{1}{k} \left[ \frac{\eta}{1-\alpha} s_0^{1-\alpha} + \zeta \nu (1 - \alpha) \ln \left( 1 + \frac{s_0^{1-\alpha}}{\nu} \right) \right] \tag{33}$$

Bring  $\mu = \sigma |s_0|^{1-\alpha}$  into (33), and we can get:

$$\begin{aligned} t_r &= \frac{1}{k} \left[ \frac{\eta}{1-\alpha} s_0^{1-\alpha} + \zeta \nu |s_0|^{1-\alpha} (1 - \alpha) \ln \left( 1 + \frac{1}{\sigma} \right) \right] \\ &= \frac{|s_0|^{1-\alpha}}{k(1-\alpha)} \left[ \eta + \zeta (1 - \alpha) \nu \ln \left( 1 + \frac{1}{\sigma} \right) \right] \end{aligned} \tag{34}$$

It is shown that the reaching law enables the system to reach the sliding surface in a finite amount of time. When  $s$  tends to 0,  $\dot{s}$  also tends to 0, and the chattering phenomenon of the system is effectively suppressed by the reaching law.

The proof of the stability of the controller is as follows:

Select a Lyapunov function  $V_1$ ,

$$V_1 = \frac{1}{2} s_1^2 \tag{35}$$

Combining (10) with (23)–(27), the time derivative is given as:

$$\begin{aligned}
 \dot{V}_1 &= s_1 \dot{s}_1 \\
 &= s_1 [\dot{e}_1 + k_1 a_1 |e_1|^{a_1-1} \dot{e}_1 \\
 &\quad + k_2 a_2 |\dot{e}_1|^{a_2-1} (\ddot{x}_{1d} - \dot{f}_1 - g_1 u_1 + \gamma_1)] \\
 &= s_1 [\dot{e}_1 + k_1 a_1 |e_1|^{a_1-1} \dot{e}_1 \\
 &\quad + k_2 a_2 |\dot{e}_1|^{a_2-1} \left( \hat{\gamma}_1 - \gamma_1 - \frac{k |s_1|^\alpha \text{sgn}(s_1)}{k_2 a_2 |\dot{e}_1|^{a_2-1} \Phi(s_1)} - \frac{\dot{e}_1 + k_1 a_1 |e_1|^{a_1-1} \dot{e}_1}{k_2 a_2 |\dot{e}_1|^{a_2-1}} \right)] \\
 &= s_1 \left[ k_2 a_2 |\dot{e}_1|^{a_2-1} (\hat{\gamma}_1 - \gamma_1) - \frac{k |s_1|^\alpha \text{sgn}(s_1)}{\eta + \zeta \left( 1 + \frac{|s_1|^{1-\alpha}}{\nu} \right)^{-1}} \right]
 \end{aligned} \tag{36}$$

According to Remark 3, we can get:

$$\begin{aligned}
 \dot{V}_1 &= s_1 \dot{s}_1 \\
 &= - \frac{k |s_1|^{\alpha+1}}{\eta + \zeta \left( 1 + \frac{|s_1|^{1-\alpha}}{\nu} \right)^{-1}} \\
 &\leq 0
 \end{aligned} \tag{37}$$

According to the proof of Lyapunov stability theory, the state  $[x_{11}, x_{12}]^T$  of control channel 1 of the system is stable. Therefore, on the basis of the same principle, we can conclude that other control channels of the system are also stable. The aerial robot system employing the improved reaching law NFTSM controller is able to reach the designed sliding surface in a finite amount of time. Theorem 2 is proved.  $\square$

**Remark 4.** *By introducing an improved reaching law NFTSM controller, the rapid convergence characteristics of the system are guaranteed. When the system is no longer on the sliding surface, the control law guarantees the convergence characteristics of the system and effectively suppresses system chattering. The manipulator of the system will cause uncertain disturbances to the system. With the help of the improved reaching law, the strong robustness and rapid convergence of the controller are retained.*

### 5. Simulation Results

In this section, in order to demonstrate the effectiveness and practicability of the NFTSMC method based on a finite-time observer and improved approach rate, a numerical simulation of an aerial robot system subject to actuator fault and internal and external disturbances was carried out. The proposed control algorithm was simulated and verified by building a system model in MATLAB.

The selection of the main parameters of the six-rotor UAV and the manipulator is shown in Table 1:

**Table 1.** Main parameters of the aerial robot.

Parameter	Numerical Value	Implication
$m$	3.85 kg	Quality of UAV
$m_1$	0.32 kg	Quality of mechanical arm
$I_{xx}$	0.29 kg/m <sup>2</sup>	Rotational inertia around x axis
$I_{yy}$	0.29 kg/m <sup>2</sup>	Rotational inertia around y axis
$I_{zz}$	0.15 kg/m <sup>2</sup>	Rotational inertia around z axis
$g$	9.8 m/s <sup>2</sup>	Acceleration of gravity
$l$	0.36 m	UAV arm length

5.1. Observer Simulation

In the system, time-varying fault functions (38) and (39) are introduced into the control channel to simulate the actuator fault; and white noise with an upper bound  $D_i = 0.018$  is introduced to simulate the external disturbance. In the eighth second of the system's operation, the joint angle of the rope-driven manipulator changes from  $[-20^\circ, -30^\circ]^T$  to  $[20^\circ, 10^\circ]^T$ , and the trajectory of the joint in space is operated according to the Cycloidal curve. In the system, the velocity and acceleration of the movement angle of the manipulator are taken into the dynamic model (2). The torque generated by each joint in the system is calculated. The running time of the manipulator is 3 s. The influence of the torque generated by the joint motion of the manipulator on the system can be approximately described as shown in Equation (40). The performance of the observer is verified on the basis of simulation experiments on control channels 1 and 4, and a comparison with the observer described in [35].

$$\mu_1 = \begin{cases} 1, t \in [0, 6] \\ 0.5 + 0.1 \sin(0.3\pi t), t \in [6, 20] \end{cases} \tag{38}$$

$$\mu_4 = \begin{cases} 1, t \in [0, 4] \\ 0.6 + 0.1 \cos(0.3\pi t), t \in [4, 20] \end{cases} \tag{39}$$

$$\mu_2 = \mu_3 = \mu_5 = \mu_6 = 1$$

$$d_\tau = \tau_1 + \tau_2 = 0.18 \cos\left(\frac{\pi}{3}t\right), t \in [8, 11] \tag{40}$$

The relevant parameters of the observer are selected as follows:  $l_1 = 0.02, l_2 = 5, l_3 = 1.5, l_4 = 1, \lambda_1 = 3, \lambda_2 = 5$ . The simulation results are shown in Figures 2 and 3.

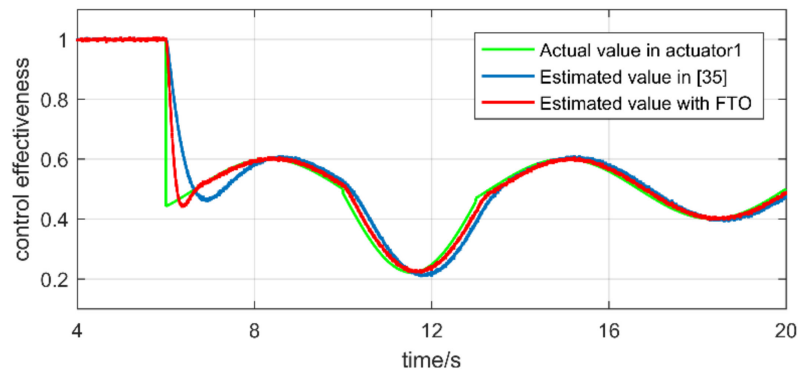


Figure 2. Observer performance comparison diagram.

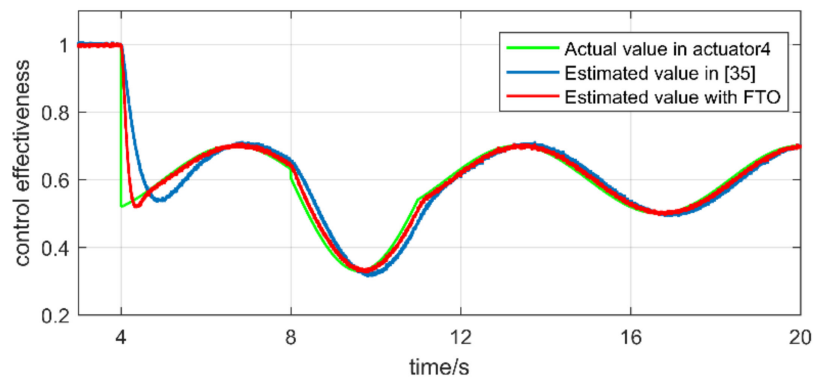


Figure 3. Observer performance comparison diagram.

By comparing the two observer channel images, the proposed observer can track the fault function curve accurately and in a timely fashion. For an abrupt actuator fault, the maximum observation error of the observer proposed in this paper is about 0.08, and the fault information of the system can be accurately tracked in about 1.3 s. For the internal disturbance of the manipulator moving in the 8th to 11th seconds, the observer proposed in this paper is about 0.5 s, and the observation error is close to zero. The simulation results of the observer described in reference [35] indicate large observation errors, and there is a certain delay in the observation of the actual value. Therefore, the proposed observer has good observation effect.

### 5.2. Simulation of Trajectory Tracking Control Effect

This section studies the control performance of an aerial robot system subjected to an actuator failure fault and internal and external disturbances. The effectiveness of the proposed control strategy is verified by inputting an actuator 10% failure fault and manipulator rotation disturbance into the system in the eighth second. We set up two sets of experiments with different initial and target conditions to verify the effectiveness of the algorithm. The first group of experiments were as follows: the initial values of the system were set as  $[x_0, y_0, z_0, \theta_0] = [0, 0.2, 0.2, -0.1]$ . The control objective was to cause the system to reach the target position within a short time  $[x_d, y_d, z_d, \theta_d] = [0.4, 0.4, 0, 0]$ . The second group of experiments was as follows: the initial values of the system were set as  $[x_0, y_0, z_0, \theta_0] = [0, 0.2, 0.6, 0.2]$ . The control objective was to cause the system to reach the target position within a short time  $[x_d, y_d, z_d, \theta_d] = [0.6, 0.8, 0, 0]$ . The initial position unit is *m* and the pitch angle unit is *rad*.

To demonstrate the superiority of the FTSMC method based on the finite-time observer and the improved reaching law, this section compares it with the SMC controller based on the traditional reaching law [34]. According to Equation (27), the parameters selected by the controller in this paper are shown in Table 2:

**Table 2.** Main parameters of the controller.

Channel	$a_1$	$a_2$	$k_1$	$k_2$	$\alpha$	$\eta$	$\zeta$	$k$
<i>x</i>	1.42	1.21	0.2	1	0.66	0.5	0.3	3.2
<i>y</i>	1.45	1.23	0.2	1	0.66	0.5	0.3	3.2
<i>z</i>	1.52	1.25	0.22	1	0.65	0.5	0.3	3.2
$\theta$	1.66	1.35	0.25	1	0.65	0.55	0.4	3.25

The simulation results are as follows:

Figures 4–11 show the tracking curves of the control strategy and the traditional sliding mode control when the system is subject to actuator faults and internal and external disturbances. Figures 4–7 show the first set of experimental data, Figures 8–11 show the second set of experimental data. The pitch angle tracking curve is shown in Figures 7 and 11.

On the basis of the first set of experiments, it can be seen from the simulation results that the proposed method enables the attitude tracking curve to reach a steady state in about 1.7 s, and the position tracking curve to reach a steady state in about 2.3 s. At the 8th s, the system fault and internal and external disturbances occurred, and the attitude system was able to effectively handle the system fault and the manipulator disturbance action after about 1.5 s. At 1.4 s, the system was stable, and the maximum vibration amplitude of the curve was 0.0052 rad. The position system was able to achieve stability after about 2.5 s. At the 10th s, the attitude system was able to achieve stability in 1.2 s or so, and the maximum amplitude of the curve was 0.0036 rad; the position system was able to reach a steady state in 1.5 s. The conclusion of the second group of experiments is similar to that of the first group. It can be seen that in the *z*-axis attitude control, the traditional sliding mode control also has a certain effect when dealing with faults and disturbances, but our control strategy has better control effect than that of the traditional sliding mode control described in reference [36].

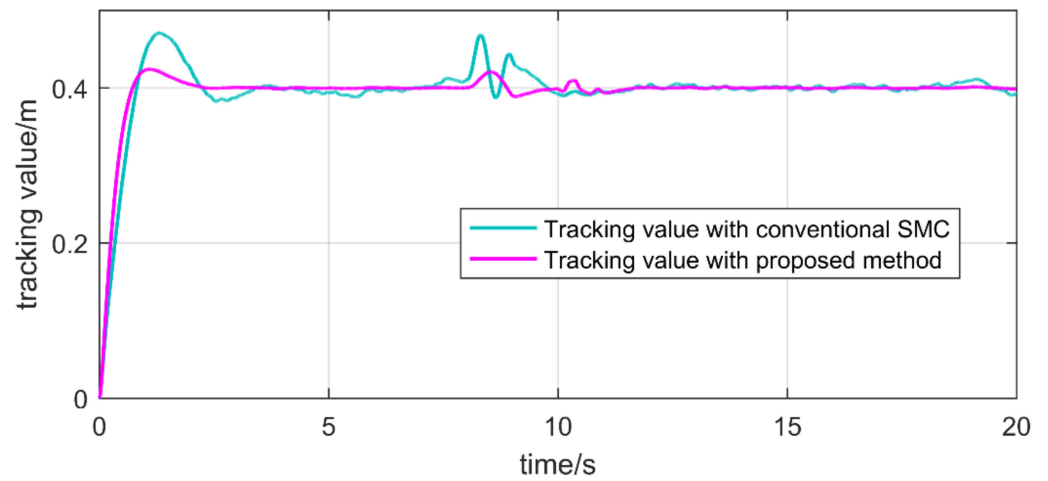


Figure 4. Trajectory tracking of position  $x$ .

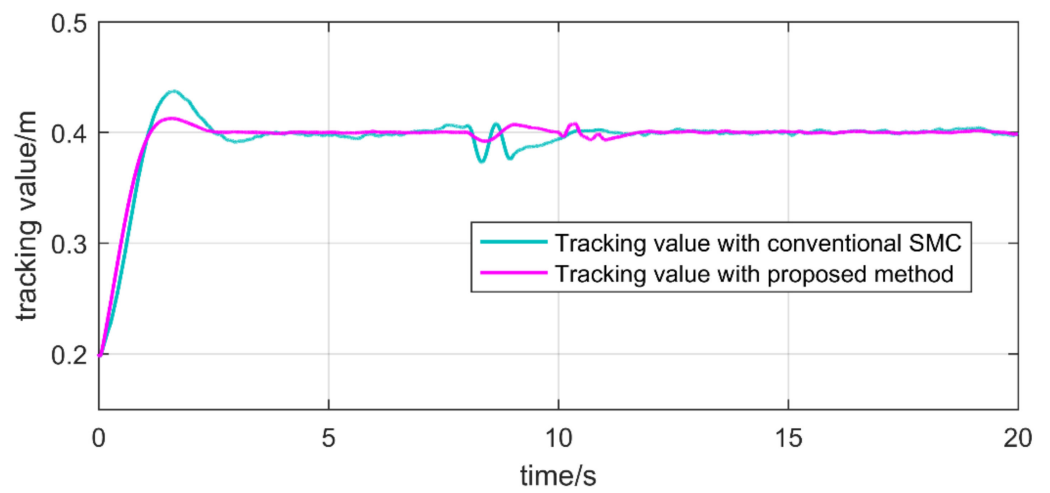


Figure 5. Trajectory tracking of position  $y$ .

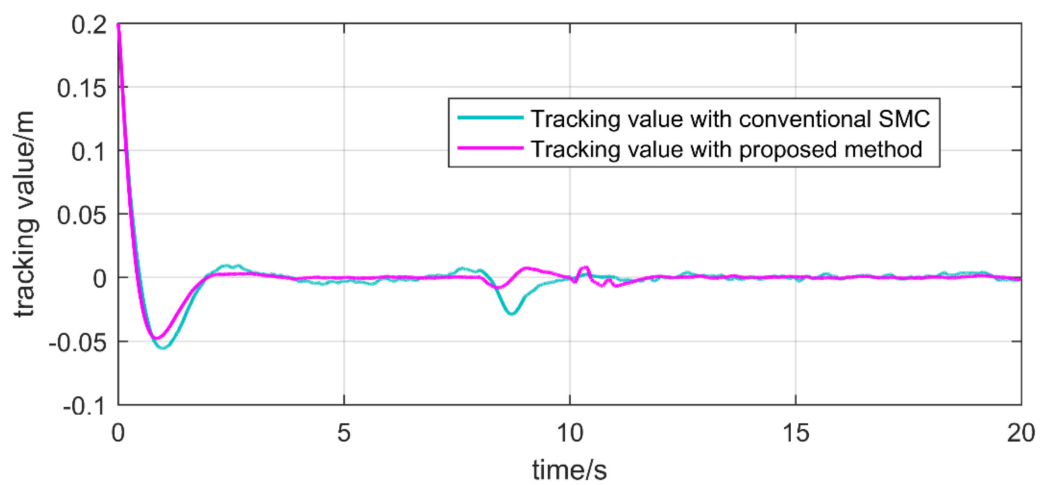


Figure 6. Trajectory tracking of position  $z$ .

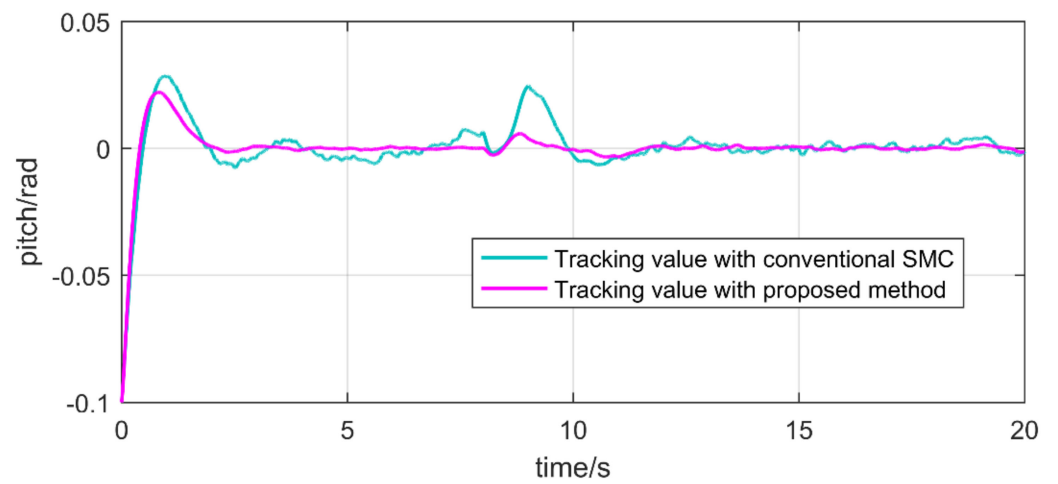


Figure 7. The tracking value of pitch.

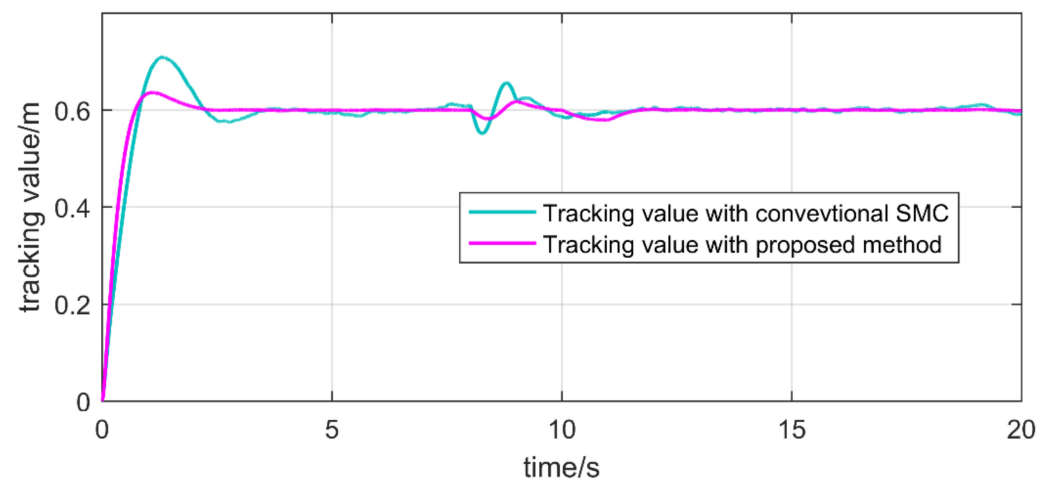


Figure 8. Trajectory tracking of position  $x$ .

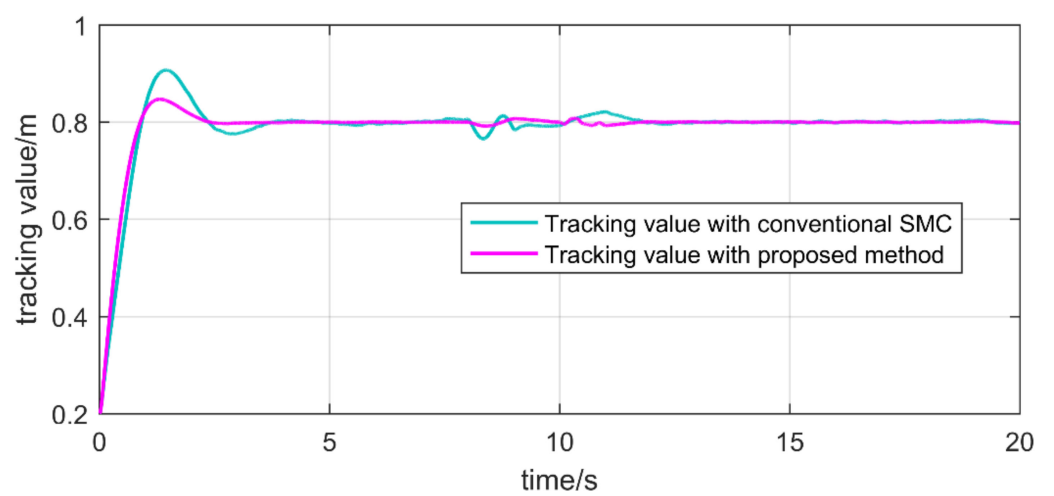


Figure 9. Trajectory tracking of position  $y$ .

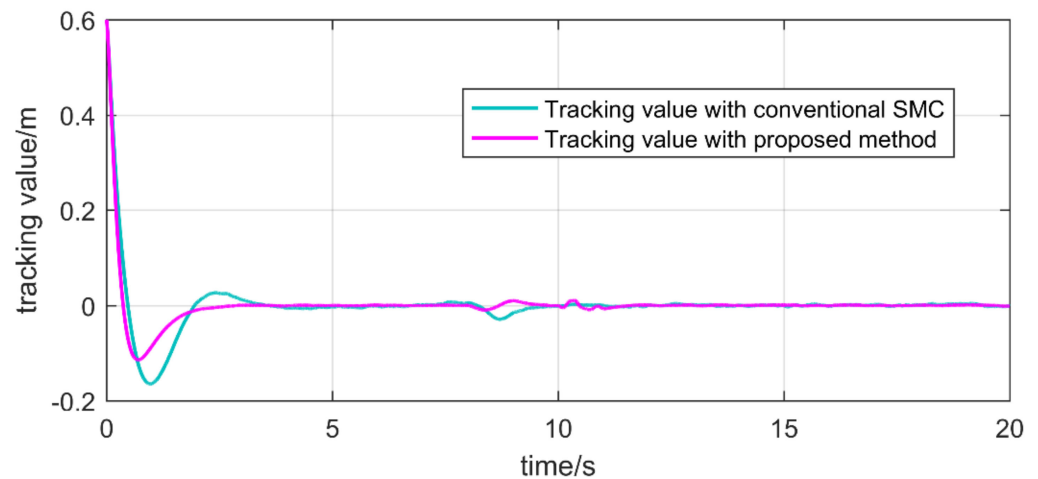


Figure 10. Trajectory tracking of position  $z$ .

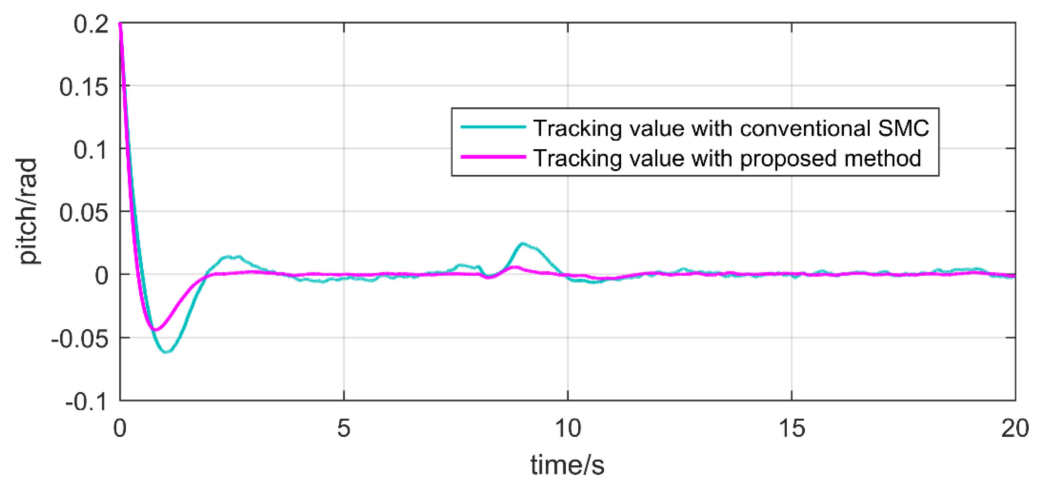


Figure 11. The tracking value of pitch.

The traditional sliding mode control method is able to make the system stable, but there are some defects. First, with respect to the position and attitude tracking process of the system, the overshoot and adjustment time of the proposed method are small. Secondly, the proposed method is able to effectively suppress the chattering of the system, while the traditional sliding mode control cannot. Finally, when the actuator faults and internal and external disturbances occur simultaneously, the method proposed in this paper is able to quickly stabilize the system, while the traditional sliding mode causes severe system jitter, and the adjustment time is large.

On the basis of the above comparative analysis, it can be seen that the proposed control strategy has better tracking performance and higher accuracy with respect to stability.

## 6. Conclusions

In this paper, a non-singular fast terminal sliding mode control algorithm based on a finite-time observer and improved reaching rate was proposed for aerial robot systems that are subject to actuator faults, manipulators, and external noise disturbances. The introduction of a finite observer was able to accurately and quickly diagnose faults and obtain disturbance information in the system, thus providing the control strategy for the controller. The introduction of improved reaching rate effectively suppresses the chattering phenomenon of the system and improves the control accuracy of the system. When the system reaches the sliding surface, the coefficient of the discontinuous switching function of the non-singular fast terminal sliding mode controller guarantees the robustness of the

system by maintaining a large slope, and it has faster convergence characteristics than the traditional terminal sliding mode control.

In the face of actuator faults and internal and external disturbances of the system, the controller proposed in this paper has high robustness and anti-interference ability. Therefore, this controller can be used in other models with higher anti-interference requirements. The simulation and experiment performed using the aerial robot model demonstrate the effectiveness of the proposed control strategy. In future research, the motion control problem of the manipulator of the aerial robot will be considered in three-dimensional space, not just in the plane.

**Author Contributions:** Conceptualization, P.Y.; methodology, P.Y. and K.F.; validation, K.F.; formal analysis, K.F.; investigation, Y.D. and Z.S.; writing—original draft preparation, K.F.; writing—review and editing, K.F., Y.D. and Z.S.; supervision, P.Y. All authors have read and agreed to the published version of the manuscript.

**Funding:** This work is supported by National Key Laboratory of Science and Technology on Helicopter Transmission (Grant No. HTL-O-21G11), the Aeronautical Science Foundation of China (20200007018001), the Aero Engine Corporation of China Industry-University-Research cooperation project (HFZL2020CXY011) and the Research Fund of State Key Laboratory of Mechanics and Control of Mechanical Structures (Nanjing University of Aeronautics and Astronautics) (MCMS-I-0121G03).

**Data Availability Statement:** Not applicable.

**Conflicts of Interest:** The authors declare no conflict of interest.

## References

1. Yates, M.; Hart, G.; Houghton, R.; Torres, M.T.; Pound, M. Evaluation of synthetic aerial imagery using unconditional generative adversarial networks. *ISPRS J. Photogramm. Remote Sens.* **2022**, *190*, 231–251. [[CrossRef](#)]
2. Cho, S.W.; Park, H.J.; Lee, H.; Shim, D.H.; Kim, S. Coverage path planning for multiple unmanned aerial vehicles in maritime search and rescue operations. *Comput. Ind. Eng.* **2021**, *161*, 107612. [[CrossRef](#)]
3. Amin, B.; Valerio, M.; Giuseppe, S.; Muhammad, A.; Luigi, I.; Luigi, G. A survey on the application of path-planning algorithms for multi-rotor UAVs in precision agriculture. *J. Navig.* **2022**, *75*, 364–383.
4. Satoshi, O.; Ohara, K.; Ikeda, T.; Ichikawa, A.; Asizawa, S.; Oomichi, T.; Fukuda, T. Light weight manipulator on UAV system for infrastructure inspection. In Proceedings of the MHS International Symposium on Micro-NanoMechatronics and Human Science, Nagoya, Japan, 9–12 December 2018; pp. 1–3.
5. Kocer, B.B.; Tjahjowidodo, T.; Seet, G.G.L. Model predictive UAV-tool interaction control enhanced by external forces. *Mechatronics* **2019**, *58*, 47–57. [[CrossRef](#)]
6. Boon, H.; Bahadir, K.B.; Mirko, K. Vision based crown loss estimation for individual trees with remote aerial robots. *ISPRS J. Photogramm. Remote Sens.* **2022**, *188*, 75–88.
7. Thomas, J.; Loianno, G.; Daniilidis, K.; Kumar, V. Visual servoing of Quadrotors for perching by hanging from cylindrical objects. *IEEE Robot. Autom. Lett.* **2016**, *1*, 57–64. [[CrossRef](#)]
8. Ikeda, T.; Yasui, S.; Minamiyama, S.; Ohara, K.; Ashizawa, S.; Ichikawa, A.; Okino, A.; Oomichi, T.; Fukuda, T. Stable impact and contact force control by UAV for inspection of floor slab of bridge. *Adv. Robot.* **2018**, *32*, 1061–1076. [[CrossRef](#)]
9. Ollero, A.; Tognon, M.; Suarez, A.; Lee, D.; Franchi, A. Past Present and Future of Aerial Robotic Manipulators. *IEEE Trans. Robot.* **2021**, *38*, 626–645. [[CrossRef](#)]
10. Garcia-Aunon, P.; Cruz, A.B. Control optimization of an aerial robotic swarm in a search task and its adaptation to different scenarios. *J. Comput. Sci.* **2018**, *29*, 107–118. [[CrossRef](#)]
11. Shi, F.; Zhao, M.; Anzai, T.; Ito, K.; Chen, X.; Nozawa, S.; Okada, K.; Inaba, M. Multi-rigid-body dynamics and online model predictive control for transformable multi-links aerial robot. *Adv. Robot.* **2019**, *33*, 971–984. [[CrossRef](#)]
12. Guo, D.; Bourne, J.R.; Wang, H.; Yim, W.; Leang, K.K. Adaptive-Repetitive Visual-Servo Control of Low-Flying Aerial Robots via Uncalibrated High-Flying Cameras. *J. Nonlinear Sci.* **2017**, *27*, 1235–1256. [[CrossRef](#)]
13. Chirarattananon, P.; Ma, K.Y.; Wood, R.J. Perching with a robotic insect using adaptive tracking control and iterative learning control. *Int. J. Robot. Res.* **2016**, *35*, 1185–1206. [[CrossRef](#)]
14. Jafarinasab, S.; Sirouspour, S.; Dyer, E. Model-based motion control of a robotic manipulator with a flying multirotor base. *IEEE/ASME Trans. Mechatron.* **2019**, *24*, 2328–2340. [[CrossRef](#)]
15. Tognon, M.; Dash, S.S.; Franchi, A. Observer-based control of position and tension for an aerial robot tethered to a moving platform. *IEEE Robot. Autom. Lett.* **2016**, *1*, 732–737. [[CrossRef](#)]
16. San-Miguel, A.; Puig, V.; Alenyà, G. Disturbance observer-based LPV feedback control of a N-DoF robotic manipulator including compliance through gain shifting. *Control Eng. Pract.* **2021**, *115*, 104887. [[CrossRef](#)]

17. Wang, B.; Yu, X.; Mu, L.; Zhang, Y. Disturbance observer-based adaptive fault-tolerant control for a quadrotor helicopter subject to parametric uncertainties and external disturbances. *Mech. Syst. Signal Processing* **2019**, *120*, 727–743. [[CrossRef](#)]
18. Wilmsen, M.; Yao, C.; Schuster, M.; Li, S.; Janschek, K. Nonlinear Wrench Observer Design for an Aerial Manipulator. *IFAC-PapersOnline* **2019**, *52*, 1–6. [[CrossRef](#)]
19. Orsag, M.; Korpela, C.; Bogdan, S.; Oh, P. Dexterous aerial robots-Mobile manipulation using unmanned aerial systems. *IEEE Trans. Robot.* **2017**, *33*, 1453–1466. [[CrossRef](#)]
20. Pounds, P.E.I.; Dollar, A.M. Stability of helicopters in compliant contact under PD-PID control. *IEEE Trans. Robot.* **2014**, *30*, 1472–1486. [[CrossRef](#)]
21. Seyedtabaai, S. New flat phase margin fractional order PID design: Perturbed UAV roll control study. *Robot. Auton. Syst.* **2017**, *96*, 58–64. [[CrossRef](#)]
22. Wang, Y.; Shi, Y.; Cai, M.; Xu, W.; Yu, Q. Optimization of air–fuel ratio control of fuel-powered UAV engine using adaptive fuzzy-PID. *J. Frankl. Inst.* **2018**, *355*, 8554–8575. [[CrossRef](#)]
23. Fan, W.; Xu, B.; Zhang, Y.; Tang, S.; Xiang, C. Adaptive fault-tolerant control of a novel ducted-fan aerial robot against partial actuator failure. *Aerosp. Sci. Technol.* **2022**, *122*, 107371. [[CrossRef](#)]
24. Jin, Z.; Wu, J.; Liu, A.; Zhang, W.; Yu, L. Gaussian process-based nonlinear predictive control for visual servoing of constrained mobile robots with unknown dynamics. *Robot. Auton. Syst.* **2021**, *136*, 103712. [[CrossRef](#)]
25. Rodríguez, O.; Ornelas, F.; Ramírez, A.; Hurtado-Ramos, J.B.; González-Barbosa, J.J. Backstepping control for a UAV-manipulator tuned by Cuckoo Search algorithm. *Robot. Auton. Syst.* **2022**, *147*, 103910. [[CrossRef](#)]
26. Chandra, A.; Lal, P.P.S. Higher order sliding mode controller for a Quadrotor UAV with a suspended load. *IFAC-PapersOnLine* **2022**, *55*, 610–615. [[CrossRef](#)]
27. Zhao, J.; Wang, Y.; Wang, D.; Ju, F.; Chen, B.; Wu, H. Practical continuous nonsingular terminal sliding mode control of a cable-driven manipulator developed for aerial robots. *Proc. Inst. Mech. Eng. Part I J. Syst. Control Eng.* **2020**, *234*, 1011–1023. [[CrossRef](#)]
28. Camci, E.; Kripalani, D.R.; Ma, L.; Kayacan, E.; Khanesar, M.A. An aerial robot for rice farm quality inspection with type-2 fuzzy neural networks tuned by particle swarm optimization-sliding mode control hybrid algorithm. *Swarmand Evol. Comput.* **2018**, *41*, 1–8. [[CrossRef](#)]
29. Ding, X.; Guo, P.; Xu, K.; Yu, Y. A review of aerial manipulation of small-scale rotorcraft unmanned robotic systems. *Chin. J. Aeronaut.* **2018**, *32*, 200–214. [[CrossRef](#)]
30. Omar, A.; Jasim, S.M.; Veres, A. Robust controller for multi rotor UAVs. *Aerosp. Sci. Technol.* **2020**, *105*, 106010.
31. Li, S.; Wang, H.; Rafique, M.U. A Novel Recurrent Neural Network for Manipulator Control with Improved Noise Tolerance. *IEEE Trans. Neural Netw. Learn. Syst.* **2018**, *29*, 1908–1918. [[CrossRef](#)]
32. Yang, P.; Wang, Z.; Zhang, Z.; Hu, X. Sliding Mode Fault Tolerant Control for a Quadrotor with Varying Load and Actuator Fault. *Actuators* **2021**, *10*, 323. [[CrossRef](#)]
33. Jin, X. Adaptive fixed-time control for MIMO nonlinear systems with asymmetric output constraints using universal barrier functions. *IEEE Trans. Autom. Control.* **2019**, *64*, 3046–3053. [[CrossRef](#)]
34. Qiao, N.; Wang, L.; Liu, M.; Wang, Z. The sliding mode controller with improved reaching law for harvesting robots. *J. Intell. Robot. Syst.* **2022**, *104*, 9. [[CrossRef](#)]
35. Wu, X.; Luo, S.; Wei, C.; Liao, Y. Observer-based fault-tolerant attitude tracking control for rigid spacecraft with actuator saturation and faults. *Acta Astronaut.* **2021**, *178*, 824–834. [[CrossRef](#)]
36. Ding, Y.; Wang, X.; Bai, Y.; Cui, N. Global smooth sliding mode controller for flexible air-breathing hypersonic vehicle with actuator faults. *Aerosp. Sci. Technol.* **2019**, *92*, 563–578. [[CrossRef](#)]